Title
Enhanced Thermal Conductivity in a Diamine-Appended Metal–Organic Framework as a Result of Cooperative CO2 Adsorption

Journal
ACS Applied Materials & Interfaces, 12(40)

ISSN
1944-8244

Authors
Babaei, Hasan
Lee, Jung-Hoon
Dods, Matthew N
et al.

Publication Date
2020-10-07

DOI
10.1021/acsami.0c10233

Peer reviewed

Enhanced Thermal Conductivity in a Diamine-Appended Metal–Organic Framework as a Result of Cooperative CO_2 Adsorption

Hasan Babaei,[a]* Jung-Hoon Lee,[b] Matthew N. Dods,[c] Christopher E. Wilmer,[d] and Jeffrey R. Long[a,c,e]

[a]Department of Chemistry, University of California, Berkeley, California 94720, United States

[b]Computational Science Research Center, Korea Institute of Science and Technology (KIST), Seoul 02792, Republic of Korea

[c]Department of Chemical and Biomolecular Engineering, University of California, Berkeley, California 94720, United States

[d]Department of Chemical & Petroleum Engineering, University of Pittsburgh, 3700 O'Hara St, Pittsburgh, PA, 15261

[e]Materials Sciences Division, Lawrence Berkeley National Laboratory, Berkeley, California 94720, United States

*Corresponding author. E-mail address: hasan.babaei@berkeley.edu

Abstract

Diamine-appended variants of the metal–organic framework M_2(dobpdc) (M = Mg, Mn, Fe, Co, Zn; dobpdc^{4-} = 4,4′-dioxidobiphenyl-3,3′-dicarboxylate) exhibit exceptional CO_2 capture properties owing to a unique cooperative adsorption mechanism, and thus hold promise for use in the development of energy- and cost-efficient CO_2 separations. Understanding the nature of thermal transport in these materials is essential for such practical applications, however, as temperature rises resulting from exothermic CO_2 uptake could potentially off-set the energy savings offered by such cooperative adsorbents. Here, molecular dynamics simulations are employed in investigating thermal transport in bare and e-2-appended Zn_2(dobpdc) (e-2 = *N*-ethylethylenediamine), both with and without CO_2 as a guest. In the absence of CO_2, the appended diamines function to enhance thermal conductivity in the *ab*-plane of e-2–Zn_2(dobpdc) relative to the bare framework, as a result of non-covalent interactions between adjacent diamines that provide additional heat transfer pathways across the pore channel. Upon introduction of CO_2, the thermal conductivity along the pore channel (the *c*-axis) increases due to the cooperative formation of metal-bound ammonium carbamates, which serve to create additional heat transfer pathways. In contrast, the thermal conductivity of the bare framework remains unchanged in the presence of zinc-bound CO_2 but decreases in the presence of additional adsorbed CO_2.

Keywords: Metal-organic framework, diamine-M_2(dobpdc), heat transfer, CO_2 capture, phonon scattering

Introduction

Metal–organic frameworks are crystalline, porous solids that exhibit vast chemical and structural tunability, and in tandem with their extremely high internal surface areas, these properties have rendered them promising candidates for a variety of applications, including gas storage, molecular separations, and catalysis.[1–5] Recently, diamine-appended frameworks with the formula $(diamine)_2M_2(dobpdc)$ (also known as diamine–M_2(dobpdc); M = Mg, Mn, Fe, Co, Zn; $dobpdc^{4-}$ = 4,4′-dioxidobiphenyl-3,3′-dicarboxylate) have been shown to capture CO_2 with unprecedented efficiency and selectivity.[6–13] In these materials, CO_2 reacts with the metal-bound amine to form a metal-bound ammonium carbamate, which then propagates as ion-paired ammonium carbamate chains that extend along the framework channels.[7,9,14] Single-crystal X-ray diffraction structures of Zn_2(dobpdc), e-2–Zn_2(dobpdc) (e-2 = *N*-ethylethylenediamine), and e-2–Zn_2(dobpdc)–CO_2 are shown in Fig. 1, as determined in Ref. [9]. This unique mechanism gives rise to step-shaped CO_2 uptake, and the material step temperature (isobaric conditions) or step pressure (isothermal conditions) can be tuned based on the choice of appended diamine. As such, these materials are of interest for various challenging separations in industry, including the capture of CO_2 from power plant flue emissions,[7,9,11,15] as they can operate using much smaller pressure or temperature swings and achieve higher working capacities than traditional adsorbents.

One important practical consideration in evaluating the performance of these materials is the rate at which CO_2 can be loaded into the pores without causing a prohibitively sharp temperature increase. Indeed, adsorption of CO_2 is an exothermic process, potentially leading to a considerable increase in the local temperature that is higher than the step temperature in an adsorption isobar curve. To dissipate this heat quickly and maximize the quantity of CO_2 adsorbed, a given framework must have a high thermal conductivity. Additionally, high thermal conductivities can reduce adsorption/desorption cycle times in practical configurations, which can lead to improvements in process efficiency. Previous investigations of thermal transport in MOFs have predominantly been limited to materials in the absence of guest molecules,[16–22] while the few studies that have investigated heat transfer in the presence of an adsorbed gas have considered only physisorbed gases.[23–25] Our previous studies[23,25,26] have shown that the presence of physisorbed guests introduces new phonon scattering channels resulting from gas-framework collisions, which serve to reduce thermal conductivity. The possible effects of chemisorbed guests on thermal transport in MOFs, however, have remained unstudied.

In this work, we use molecular dynamics (MD) simulations to investigate mechanisms of heat transfer in bare and e-2-appended Zn_2(dobpdc) (e-2 = *N*-ethylethylenediamine), and we apply the Green-Kubo method to predict their thermal conductivities with and without adsorbed CO_2. Consistent with our previous studies, thermal conductivity in the bare material is diminished in the presence of (non-coordinating) physisorbed CO_2, whereas it is unchanged in the presence of more strongly adsorbed, zinc-bound CO_2. Importantly, however, an enhancement in thermal conductivity is observed for e-2–Zn_2(dobpdc) upon chemisorption of CO_2, resulting from the introduction of new heat transfer pathways along the framework channels. This result is in contrast to the reduction in thermal conductivity that occurs in the presence of physisorbed guests and has important implications for heat management during CO_2 adsorption that is of relevance for practical separation applications.

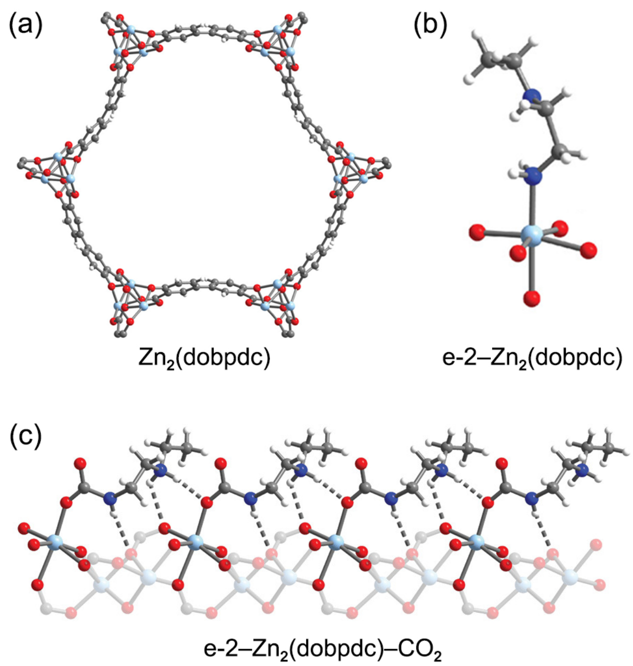

Fig. 1. (a) Portion of the single-crystal X-ray diffraction structure of Zn_2(dobpdc) viewed down the framework channel (*c* axis); (b) a view of the primary coordination sphere of a zinc(II) node in the dominant conformation of e-2–Zn_2(dobpdc); and (c) crystal structure of the dominant conformation of e-2–Zn_2(dobpdc) following cooperative CO_2 insertion into the metal–amine bonds, which results in the formation of chains of ammonium carbamate that propagate along the channel direction. Images were adapted from Ref. [9]; light blue, red, dark blue, gray, and white spheres represent Zn, O, N, C, and H atoms, respectively. Thermal transport in all three frameworks was investigated in this work using molecular dynamics simulations.

Structures and Methodology

In our calculations, we evaluated the thermal conductivity of guest-free Zn_2(dobpdc) and e-2–Zn_2(dobpdc), e-2–Zn_2(dobpdc) with chemisorbed CO_2, and Zn_2(dobpdc) in the presence of metal-bound and more weakly physisorbed CO_2. In the case of Zn_2(dobpdc), metal-bound CO_2 molecules do not move from their initial DFT-determined locations in the pores, whereas the other more weakly associated physisorbed CO_2 molecules are those that can diffuse away from their initial random calculated positions. The simulation cell size for each framework was set based on the DFT-relaxed lattice constants. For the interactions between atoms in Zn_2(dobpdc), e-2–Zn_2(dobpdc) and e-2–Zn_2(dobpdc)–CO_2, we used a modified version of the DREIDING force field,[27] in which the equilibrium distances between atoms were adjusted to the DFT-relaxed structures. Among other general force fields, we picked DREIDING as it allows for the description of existing hydrogen bonds. The required charges on atoms were obtained using the DDEC algorithm,[28] wherein partial atomic charges are calculated using the electron densities obtained from DFT calculations. The CO_2 molecules loaded within Zn_2(dobpdc) were modeled using the TraPPE force field.[29] The initial atomic configurations for the MD simulations involving metal-bound CO_2 adsorbed in Zn_2(dobpdc) were taken from snapshots of equilibrated DFT calculations.

For the DFT calculations, we used a plane-wave basis and projector augmented-wave (PAW)[30,31] pseudopotential with the Vienna ab-initio Simulation Package (VASP) code.[32–35] To include the effect of the van der Waals (vdW) dispersive interactions on binding energies and mechanical properties, we performed structural relaxations with a vdW dispersion-corrected functional (vdW-DF2)[36] as implemented in VASP. For all calculations, a Γ-point sampling of the Brillouin zone and a 600-eV plane-wave cutoff energy were employed. We explicitly treated twelve valence electrons for Zn ($3d^{10}4s^2$), six for O ($2s^22p^4$), five for N ($2s^22p^3$), four for C ($2s^22p^2$), and one for H ($1s^1$). All structural relaxations were performed with a Gaussian smearing of 0.05 eV.[37] The ions were relaxed until the Hellmann-Feynman forces were less than 0.02 eVÅ^{-1}.

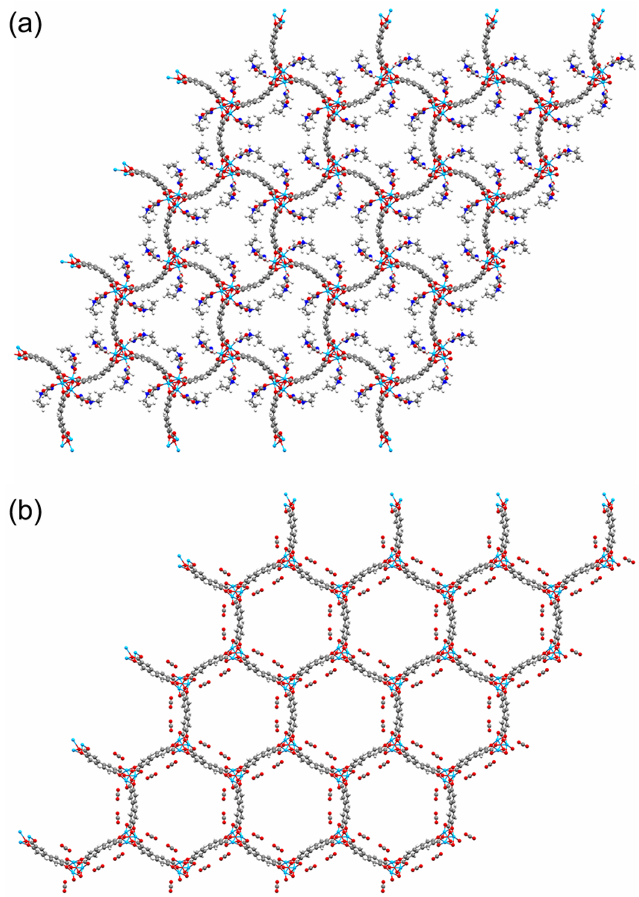

Fig. 2 Simulation box with 4×4×6 unit cells (in crystallographic directions *a*, *b* and *c*) of (a) e-2–Zn_2(dobpdc)–CO_2 and (b) CO_2 bound at the open Zn^{2+} sites within Zn_2(dobpdc). Light blue, red, blue, gray, and light gray spheres represent Zn, O, N, C, and H atoms, respectively.

The Green-Kubo method was applied to predict thermal conductivity.[38] This method involves calculating the instantaneous heat flux in an equilibrium MD simulation. The partial enthalpy terms required to analyze multicomponent systems were implemented as discussed in Refs. [[23,25,39,40]]. The MD simulations were performed using a version of the Large-scale Atomic/Molecular Massively Parallel Simulator[41] software, which can correctly implement heat flux for many-body potentials.[42] To gain further insight into the thermal conductivity predictions, we also calculated the corrected diffusivity (which is associated with molecular mobility) of metal-bound CO_2 in Zn_2(dobpdc).[43] The corrected diffusivity is based on a Green-Kubo relation and is defined as the time integral of the center of mass velocity autocorrelation function for the gas component. Details of the Green-Kubo calculations for both thermal conductivity and diffusivity are provided in the Supporting Information. For determining thermal conductivity, a system size of 4×4×6 (in crystallographic directions *a*, *b*, and *c*) unit cells was used. See Fig. 2 for snapshots of the simulation cells for e-2–Zn_2(dobpdc)–CO_2 and Zn_2(dobpdc) with metal-bound CO_2. The systems were initially equilibrated under *NPT* (constant pressure-constant temperature) conditions at a temperature of 300 K and atmospheric pressure for 500,000 time steps; under *NVT* (constant volume-constant temperature) conditions at a temperature of 300 K for 300,000 time steps; and for 200,000 time steps under *NVE* (constant volume-constant energy) conditions. Finally, *NVE* simulations were run for an additional 1,000,000 time steps where the heat current was calculated every five time steps. For all cases, this procedure was performed for four simulations starting from random velocity distributions.

Results and Discussion

Predicted thermal conductivities in the crystallographic *a*, *b*, and *c* directions are shown in Fig. 3. In all cases, thermal conductivities in the *a* and *b* directions (perpendicular to the framework channels) are the same, indicating isotropy in the *ab*-plane. Relative to the bare framework, the introduction of the metal-bound diamine increases the thermal conductivity in the *ab*-plane, from 0.4 W m^{-1} K^{-1} for Zn_2(dobpdc) to 0.5 W m^{-1} K^{-1} for e-2–Zn_2(dobpdc). In contrast, thermal conductivity decreases slightly in the *c*-direction for e-2–Zn_2(dobpdc) relative to Zn_2(dobpdc). The increase in *ab*-plane thermal conductivity can be ascribed to the presence of van der Waals interactions between diamines, which create additional heat conduits between adjacent metal nodes. However, the diamines do not interact with each other along the *c*-axis, and in this direction, they likely act instead as a phonon scattering source.

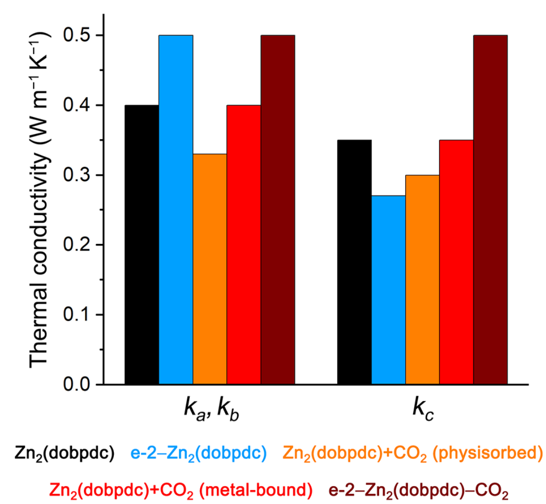

Fig. 3 Calculated thermal conductivities of Zn_2(dobpdc) and e-2-Zn_2(dobpdc) with and without CO_2 loading. The parameters k_a, k_b, and k_c correspond to the crystallographic *a*, *b*, and *c* direction as discussed in the text.

The introduction of metal-bound CO_2 in Zn_2(dobpdc) has no effect on the thermal conductivity. Molecules of CO_2 initially positioned in the vicinity of the metal nodes (suggested by DFT calculations) do not function as phonon scatterers or as agents for heat conduction. The calculated corrected diffusivities in all directions are zero, indicating that CO_2 molecules in this initial configuration do not move through the channel space. Consistent with our previous reports,[23,25] the presence of more weakly physisorbed CO_2 results in a decrease in the thermal conductivity of Zn_2(dobpdc) in all directions, as a result of gas-framework collisions and resulting phonon scattering.

In stark contrast to both scenarios for bare Zn_2(dobpdc), chemisorption of CO_2 in e-2–Zn_2(dobpdc) results in a 100% *increase* in thermal conductivity in the *c*-direction, to 0.5 W m^{-1} K^{-1}. Here, the newly-formed hydrogen-bonded ammonium carbamate chains (see Fig. 1c) provide an additional heat transfer pathway along the framework channels. The thermal conductivity of e-2–Zn_2(dobpdc)–CO_2 is notably 2-3 times higher than that of conventional activated carbon[44] and comparable to that of zeolites MFI and MEL,[45,46] which are extensively deployed in gas storage and separation applications. Importantly, as a result of this enhanced thermal conductivity upon CO_2 adsorption, less active cooling of e-2–Zn_2(dobpdc) would be required in a practical separations process. Thus, in addition to the other advantages offered by diamine-appended MOFs compared to traditional adsorbents, these materials are capable of reducing unwanted thermal effects by quickly dissipating heat generated during adsorption.

It is important to note that the thermal conductivity enhancements reported here were observed for the MOF single crystal. Changes in thermal conductivity upon chemisorption of CO_2 for corresponding bulk powder or pellet samples are expected to differ due to the presence of voids between individual crystallites which reduce thermal conductivity by introducing interfacial thermal resistance between crystallites. Future studies would benefit from an evaluation of the differences in thermal conductivity in single crystal, powder, and pellet samples upon chemisorption of CO_2. We also note that the substantial increase in thermal conductivity observed here for the diamine-appended Zn_2(dobpdc) upon CO_2 uptake is a phenomenon that is more likely to be observed for frameworks with larger pores, wherein suitable void space remains even upon incorporation of appended diamines and chemisorption products, such that there is no significant enhancement in crystal gas collisions that diminish thermal conductivity.[25] Indeed, Zn_2(dobpdc) has much larger pores and also a lower thermal conductivity than denser MOFs such as $Cu_3(BTC)_2$

(also known as HKUST-1; BTC^{3-} = 1,3,5-benzenetricarboxylate)[26] and $Zn_4O(BDC)_3$ (also known as IRMOF-1 or MOF-5; BDC^{2-} = 1,4-benzenedicarboxylate)[17], and therefore the introduction of diamines and ammonium carbamates along the *c*-axis is anticipated to result in more pronounced changes to thermal conductivity.

Conclusion

In summary, we have used MD simulations to investigate thermal transport in the frameworks Zn_2(dobpdc) and e-2–Zn_2(dobpdc) both without and with CO_2 as a guest. We find that in the presence of CO_2, the unique chemisorption mechanism in e-2–Zn_2(dobpdc) serves to enhance the thermal conductivity in the direction of the framework channels, whereas adsorption of CO_2 in the bare material has no effect on or decreases the thermal conductivity. These results point to enhanced thermal management as an additional advantage of these diamine-appended materials for practical applications. Indeed, upon CO_2 uptake, most diamine–M_2(dobpdc) frameworks follow a similar mechanism of ammonium carbamate chain formation. However, we note that certain other appended diamines, such as 2,2-dimethyl-1,3-diaminopropane, have been shown to react with CO_2 via a more complex mechanism that also involves the formation of carbamic acid pairs.[11] In the future, we plan to investigate the effects of these differing chemisorption mechanisms on thermal transport in diamine–M_2(dobpdc) frameworks.

Notes

The authors declare the following competing financial interest: J.R.L. has a financial interest in Mosaic Materials, Inc., a start-up company working to commercialize metal–organic frameworks of the type investigated here for CO_2 separations.

Acknowledgements

We gratefully acknowledge support from the National Science Foundation (NSF) awards CBET-1804011 and OAC-1931436, as well as computational resources provided by the Molecular Graphics and Computation Facility within the College of Chemistry at the University of California, Berkeley. The contributions of J.R.L. were supported by the United States Department of Energy, Office of Science, Office of Basic Energy Sciences under Award DE-SC0019992. J.-H.L.'s work was supported by the KIST Institutional Program (Project No. 2E29910). J.H.L. also acknowledges computational resources provided by KISTI Supercomputing Centre (Project No. KSC-2019-CRE-0149). We thank Dr. K. R. Meihaus for editorial assistance.

Supporting Information. Additional information on simulation methodology.

References

(1) Furukawa, H.; Cordova, K. E.; O'Keeffe, M.; Yaghi, O. M. The Chemistry and Applications of Metal-Organic Frameworks. *Science* **2013**, *341* (6149), 1230444. https://doi.org/10.1126/science.1230444.

(2) Lee, J.; Farha, O. K.; Roberts, J.; Scheidt, K. A.; Nguyen, S. T.; Hupp, J. T. Metal–Organic Framework Materials as Catalysts. *Chem. Soc. Rev.* **2009**, *38* (5), 1450–1459. https://doi.org/10.1039/B807080F.

(3) Kreno, L. E.; Leong, K.; Farha, O. K.; Allendorf, M.; Van Duyne, R. P.; Hupp, J. T. Metal–Organic Framework Materials as Chemical Sensors. *Chem. Rev.* **2012**, *112* (2), 1105–1125. https://doi.org/10.1021/cr200324t.

(4) Mueller, U.; Schubert, M.; Teich, F.; Puetter, H.; Schierle-Arndt, K.; Pastré, J. Metal–Organic Frameworks—Prospective Industrial Applications. *J. Mater. Chem.* **2006**, *16* (7), 626–636. https://doi.org/10.1039/B511962F.

(5) Sumida, K.; Rogow, D. L.; Mason, J. A.; McDonald, T. M.; Bloch, E. D.; Herm, Z. R.; Bae, T.-H.; Long, J. R. Carbon Dioxide Capture in Metal–Organic Frameworks. *Chem. Rev.* **2012**, *112* (2), 724–781. https://doi.org/10.1021/cr2003272.

(6) McDonald, T. M.; Lee, W. R.; Mason, J. A.; Wiers, B. M.; Hong, C. S.; Long, J. R. Capture of Carbon Dioxide from Air and Flue Gas in the Alkylamine-Appended Metal–Organic Framework Mmen-Mg2(Dobpdc). *J. Am. Chem. Soc.* **2012**, *134* (16), 7056–7065. https://doi.org/10.1021/ja300034j.

(7) McDonald, T. M.; Mason, J. A.; Kong, X.; Bloch, E. D.; Gygi, D.; Dani, A.; Crocellà, V.; Giordanino, F.; Odoh, S. O.; Drisdell, W. S.; Vlaisavljevich, B.; Dzubak, A. L.; Poloni, R.; Schnell, S. K.; Planas, N.; Lee, K.; Pascal, T.; Wan, L. F.; Prendergast, D.; Neaton, J. B.; Smit, B.; Kortright, J. B.; Gagliardi, L.; Bordiga, S.; Reimer, J. A.; Long, J. R. Cooperative Insertion of CO 2 in Diamine-Appended Metal-Organic Frameworks. *Nature* **2015**, *519* (7543), 303–308. https://doi.org/10.1038/nature14327.

(8) Planas, N.; Dzubak, A. L.; Poloni, R.; Lin, L.-C.; McManus, A.; McDonald, T. M.; Neaton, J. B.; Long, J. R.; Smit, B.; Gagliardi, L. The Mechanism of Carbon Dioxide Adsorption in an Alkylamine-Functionalized Metal–Organic Framework. *J. Am. Chem. Soc.* **2013**, *135* (20), 7402–7405. https://doi.org/10.1021/ja4004766.

(9) Siegelman, R. L.; McDonald, T. M.; Gonzalez, M. I.; Martell, J. D.; Milner, P. J.; Mason, J. A.; Berger, A. H.; Bhown, A. S.; Long, J. R. Controlling Cooperative CO2 Adsorption in Diamine-Appended Mg2(Dobpdc) Metal–Organic Frameworks. *J. Am. Chem. Soc.* **2017**, *139* (30), 10526–10538. https://doi.org/10.1021/jacs.7b05858.

(10) Forse, A. C.; Gonzalez, M. I.; Siegelman, R. L.; Witherspoon, V. J.; Jawahery, S.; Mercado, R.; Milner, P. J.; Martell, J. D.; Smit, B.; Blümich, B.; Long, J. R.; Reimer, J. A. Unexpected Diffusion Anisotropy of Carbon Dioxide in the Metal–Organic Framework Zn2(Dobpdc). *J. Am. Chem. Soc.* **2018**, *140* (5), 1663–1673. https://doi.org/10.1021/jacs.7b09453.

(11) Milner, P. J.; Siegelman, R. L.; Forse, A. C.; Gonzalez, M. I.; Runčevski, T.; Martell, J. D.; Reimer, J. A.; Long, J. R. A Diaminopropane-Appended Metal–Organic Framework Enabling Efficient CO2 Capture from Coal Flue Gas via a Mixed Adsorption Mechanism. *J. Am. Chem. Soc.* **2017**, *139* (38), 13541–13553. https://doi.org/10.1021/jacs.7b07612.

(12) Lin, Y.; Kong, C.; Chen, L. Amine-Functionalized Metal–Organic Frameworks: Structure, Synthesis and Applications. *RSC Adv.* **2016**, *6* (39), 32598–32614. https://doi.org/10.1039/C6RA01536K.

(13) Yeon, J. S.; Lee, W. R.; Kim, N. W.; Jo, H.; Lee, H.; Song, J. H.; Lim, K. S.; Kang, D. W.; Seo, J. G.; Moon, D.; Wiers, B.; Hong, C. S. Homodiamine-Functionalized Metal–Organic Frameworks with a MOF-74-Type Extended Structure for Superior Selectivity of CO2 over N2. *J. Mater. Chem. A* **2015**, *3* (37), 19177–19185. https://doi.org/10.1039/C5TA02357B.

(14) Forse, A. C.; Milner, P. J.; Lee, J.-H.; Redfearn, H. N.; Oktawiec, J.; Siegelman, R. L.; Martell, J. D.; Dinakar, B.; Porter-Zasada, L. B.; Gonzalez, M. I.; Neaton, J. B.; Long, J. R.; Reimer, J. A. Elucidating CO2 Chemisorption in Diamine-Appended Metal–Organic Frameworks. *J. Am. Chem. Soc.* **2018**, *140* (51), 18016–18031. https://doi.org/10.1021/jacs.8b10203.

(15) Siegelman, R. L.; Milner, P. J.; Forse, A. C.; Lee, J.-H.; Colwell, K. A.; Neaton, J. B.; Reimer, J. A.; Weston, S. C.; Long, J. R. Water Enables Efficient CO2 Capture from Natural Gas Flue Emissions in an Oxidation-Resistant Diamine-Appended Metal–Organic Framework. *J. Am. Chem. Soc.* **2019**, *141* (33), 13171–13186. https://doi.org/10.1021/jacs.9b05567.

(16) Huang, B. L.; McGaughey, A. J. H.; Kaviany, M. Thermal Conductivity of Metal-Organic Framework 5 (MOF-5): Part I. Molecular Dynamics Simulations. *Int. J. Heat Mass Transf.* **2007**, *50* (3–4), 393–404. https://doi.org/10.1016/j.ijheatmasstransfer.2006.10.002.

(17) Huang, B. L.; Ni, Z.; Millward, A.; McGaughey, A. J. H.; Uher, C.; Kaviany, M.; Yaghi, O. Thermal Conductivity of a Metal-Organic Framework (MOF-5): Part II. Measurement. *Int. J. Heat Mass Transf.* **2007**, *50* (3–4), 405–411. https://doi.org/10.1016/j.ijheatmasstransfer.2006.10.001.

(18) Liu, D.; Purewal, J. J.; Yang, J.; Sudik, A.; Maurer, S.; Mueller, U.; Ni, J.; Siegel, D. J. MOF-5 Composites Exhibiting Improved Thermal Conductivity. *Int. J. Hydrog. Energy* **2012**, *37* (7), 6109–6117. https://doi.org/10.1016/j.ijhydene.2011.12.129.

(19) Zhang, X.; Jiang, J. Thermal Conductivity of Zeolitic Imidazolate Framework-8: A Molecular Simulation Study. *J. Phys. Chem. C* **2013**, *117* (36), 18441–18447. https://doi.org/10.1021/jp405156y.

(20) Ming, Y.; Purewal, J.; Liu, D.; Sudik, A.; Xu, C.; Yang, J.; Veenstra, M.; Rhodes, K.; Soltis, R.; Warner, J.; Gaab, M.; Müller, U.; Siegel, D. J. Thermophysical Properties of MOF-5 Powders. *Microporous Mesoporous Mater.* **2014**, *185*, 235–244. https://doi.org/10.1016/j.micromeso.2013.11.015.

(21) Wang, X.; Guo, R.; Xu, D.; Chung, J.; Kaviany, M.; Huang, B. Anisotropic Lattice Thermal Conductivity and Suppressed Acoustic Phonons in MOF-74 from First Principles. *J. Phys. Chem. C* **2015**, *119* (46), 26000–26008. https://doi.org/10.1021/acs.jpcc.5b08675.

(22) Gunatilleke, W. D. C. B.; Wei, K.; Niu, Z.; Wojtas, L.; Ma, S.; Nolas, G. S. Thermal Conductivity of Perovskite-Type Metal-Organic Framework Crystal. *Dalton Trans.* **2017**. https://doi.org/10.1039/C7DT02927F.

(23) Babaei, H.; Wilmer, C. E. Mechanisms of Heat Transfer in Porous Crystals Containing Adsorbed Gases: Applications to Metal-Organic Frameworks. *Phys. Rev. Lett.* **2016**, *116* (2), 025902. https://doi.org/10.1103/PhysRevLett.116.025902.

(24) Han, L.; Budge, M.; Alex Greaney, P. Relationship between Thermal Conductivity and Framework Architecture in MOF-5. *Comput. Mater. Sci.* **2014**, *94*, 292–297. https://doi.org/10.1016/j.commatsci.2014.06.008.

(25) Babaei, H.; McGaughey, A. J. H.; Wilmer, C. E. Effect of Pore Size and Shape on the Thermal Conductivity of Metal-Organic Frameworks. *Chem. Sci.* **2016**, *8* (1), 583–589. https://doi.org/10.1039/C6SC03704F.

(26) Babaei, H., DeCoster, M. E., Jeong, M., Hassan, Z. M., Islamoglu, T., Baumgart, H., McGaughey, A. J. H., Engelbert, R., Farha, O. K., Hopkins, P. E., Malen, J. A. & Wilmer, C. E. Observation of Reduced Thermal Conductivity in a Metal-Organic Framework Due to the Presence of Adsorbates. *Accept. Nat. Commun.*

(27) Mayo, S. L.; Olafson, B. D.; Goddard, W. A. DREIDING: A Generic Force Field for Molecular Simulations. *J. Phys. Chem.* **1990**, *94* (26), 8897–8909. https://doi.org/10.1021/j100389a010.

(28) Manz, T. A.; Limas, N. G. Introducing DDEC6 Atomic Population Analysis: Part 1. Charge Partitioning Theory and Methodology. *RSC Adv.* **2016**, *6* (53), 47771–47801. https://doi.org/10.1039/C6RA04656H.

(29) Potoff, J. J.; Siepmann, J. I. Vapor–Liquid Equilibria of Mixtures Containing Alkanes, Carbon Dioxide, and Nitrogen. *AIChE J.* **2001**, *47* (7), 1676–1682. https://doi.org/10.1002/aic.690470719.

(30) Blöchl, P. E. Projector Augmented-Wave Method. *Phys. Rev. B* **1994**, *50*, 17953–17979.

(31) Kresse, G.; Joubert, D. From Ultrasoft Pseudopotentials to the Projector Augmented-Wave Method. *Phys. Rev. B* **1999**, *59*, 1758–1775. https://doi.org/10.1103/PhysRevB.59.1758.
(32) Kresse, G.; Hafner, J. Ab Initio Molecular Dynamics for Liquid Metals. *Phys. Rev. B* **1993**, *47*, 558–561. https://doi.org/10.1103/PhysRevB.47.558.
(33) Kresse, G.; Furthmüller, J. Efficient Iterative Schemes for Ab Initio Total-Energy Calculations Using a Plane-Wave Basis Set. *Phys. Rev. B* **1996**, *54*, 11169–11186. https://doi.org/10.1103/PhysRevB.54.11169.
(34) Kresse, G.; Furthmüller, J. Efficiency of Ab-Initio Total Energy Calculations for Metals and Semiconductors Using a Plane-Wave Basis Set. *Comput. Mater. Sci.* **1996**, *6*, 15–50. https://doi.org/10.1016/0927-0256(96)00008-0.
(35) Kresse, G.; Hafner, J. Ab Initio Molecular-Dynamics Simulation of the Liquid-Metal–Amorphous-Semiconductor Transition in Germanium. *Phys. Rev. B* **1994**, *49*, 14251–14269. https://doi.org/10.1103/PhysRevB.49.14251.
(36) Lee, K.; Murray, É. D.; Kong, L.; Lundqvist, B. I.; Langreth, D. C. A Higher-Accuracy van Der Waals Density Functional. *Phys Rev B* **2010**, *82*, 081101. https://doi.org/10.1103/PhysRevB.82.081101.
(37) Elsässer, C.; Fähnle, M.; Chan, C. T.; Ho, K. M. Density-Functional Energies and Forces with Gaussian-Broadened Fractional Occupations. *Phys. Rev. B* **1994**, *49*, 13975–13978. https://doi.org/10.1103/PhysRevB.49.13975.
(38) Schelling, P. K.; Phillpot, S. R.; Keblinski, P. Comparison of Atomic-Level Simulation Methods for Computing Thermal Conductivity. *Phys. Rev. B* **2002**, *65* (14), 144306. https://doi.org/10.1103/PhysRevB.65.144306.
(39) Babaei, H.; Keblinski, P.; Khodadadi, J. M. Equilibrium Molecular Dynamics Determination of Thermal Conductivity for Multi-Component Systems. *J. Appl. Phys.* **2012**, *112* (5), 054310. https://doi.org/10.1063/1.4749265.
(40) Babaei, H.; Keblinski, P.; Khodadadi, J. M. A Proof for Insignificant Effect of Brownian Motion-Induced Micro-Convection on Thermal Conductivity of Nanofluids by Utilizing Molecular Dynamics Simulations. *J. Appl. Phys.* **2013**, *113* (8), 084302. https://doi.org/10.1063/1.4791705.
(41) Plimpton, S. Fast Parallel Algorithms for Short-Range Molecular Dynamics. *J. Comput. Phys.* **1995**, *117* (1), 1–19. https://doi.org/10.1006/jcph.1995.1039.
(42) Boone, P.; Babaei, H.; Wilmer, C. E. Heat Flux for Many-Body Interactions: Corrections to LAMMPS. *J. Chem. Theory Comput.* **2019**, *15* (10), 5579–5587. https://doi.org/10.1021/acs.jctc.9b00252.
(43) Maginn, E. J.; Bell, A. T.; Theodorou, D. N. Transport Diffusivity of Methane in Silicalite from Equilibrium and Nonequilibrium Simulations. *J. Phys. Chem.* **1993**, *97* (16), 4173–4181. https://doi.org/10.1021/j100118a038.
(44) Menard, D.; Py, X.; Mazet, N. Activated Carbon Monolith of High Thermal Conductivity for Adsorption Processes Improvement: Part A: Adsorption Step. *Chem. Eng. Process. Process Intensif.* **2005**, *44* (9), 1029–1038. https://doi.org/10.1016/j.cep.2005.02.002.
(45) Hudiono, Y.; Greenstein, A.; Saha-Kuete, C.; Olson, B.; Graham, S.; Nair, S. Effects of Composition and Phonon Scattering Mechanisms on Thermal Transport in MFI Zeolite Films. *J. Appl. Phys.* **2007**, *102* (5), 053523. https://doi.org/10.1063/1.2776006.
(46) Greenstein, A.; Hudiono, Y.; Graham, S.; Nair, S. Effects of Nonframework Metal Cations and Phonon Scattering Mechanisms on the Thermal Transport Properties of Polycrystalline Zeolite LTA Films. *J. Appl. Phys.* **2010**, *107* (6), 063518. https://doi.org/10.1063/1.3327419.
(47) Schlemminger, C.; Næss, E.; Bünger, U. Adsorption Hydrogen Storage at Cryogenic Temperature – Material Properties and Hydrogen Ortho-Para Conversion Matters. *Int. J. Hydrog. Energy* **2015**, *40* (20), 6606–6625. https://doi.org/10.1016/j.ijhydene.2015.03.104.

TOC